PERGAMON

International Journal of Heat and Mass Transfer 45 (2002) 1173–1184

International Journal of HEAT and MASS TRANSFER

www.elsevier.com/locate/ijhmt

Modeling of heat transfer in turbulent gas–solid flow

Z. Mansoori [a], M. Saffar-Avval [a], H. Basirat Tabrizi [a], G. Ahmadi [b,*]

[a] *Mechanical Engineering Department, Amirkabir University of Technology, P.O. Box 15875-4413, Tehran, Iran*
[b] *Department of Mechanical and Aeronautical Engineering, Clarkson University, Potsdam, NY 13699-5725, USA*

Received 18 February 2001; received in revised form 6 July 2001

Abstract

The turbulent heat transfer in a vertical upward gas–solid flow is studied. The new model uses the two-way interaction of two-phase flows and an Eulerian/Lagrangian approach. The model considers the thermal turbulent field characteristics and includes k_θ–τ_θ equation model, in addition to the k–τ model for two-phase flow. Numerical model validation was performed for an upward pipe gas–solid flow with constant wall heat transfer. Variations of the heat transfer coefficient for a turbulent suspension of 200 μm sand particles at a Reynolds number of 23 000 is studied.

Keywords: Heat transfer; Gas–solid flow; k_θ–τ_θ model

1. Introduction

The interactions between solid particles and gas turbulence and thermal field often play an important role in many industrial processes. The dispersion of thermal pollutant in atmosphere and ocean, evaporation of spray droplets, and combustion of pulverized coal particles in boilers are industrial examples illustrating the importance of the thermal transport between the two phases. The interaction between gas and particle depends on many factors including gas and particle physical properties and velocities, concentration, temperatures and turbulent intensities.

While numerous experiments and numerical studies on the influence of particles on suppression/enhancement of fluid turbulence have been performed, the thermal interactions between the two phases are not as yet well understood. It is, however, known that the turbulence modulation due to the particles plays an important role in the heat transfer enhancement [1]. In the recent years, using the k–ε model, several authors reported reasonable agreement between the computational simulation and the experimental measurement [2] in the absence of heat transfer. In these earlier models, the effect of the presence of the dispersed phase is represented by extra dissipation terms in both k and ε equations. These additional terms are referred to as the particle source terms that are added to the k–ε transport equations.

Studies of particle and fluid thermal interactions are rather scarce. Han et al. [3] analyzed heat transfer of the turbulent dilute gas–particle flows numerically in a vertical pipe with constant wall heat flux. A two-fluid model using a thermal eddy diffusivity concept was proposed to model the heat transfer in the duct. They concluded that the decrease in the Nusselt number at low loading ratios is mainly due to the increase of the viscous sublayer thickness caused by the suppression of turbulence near the wall by the presence of solid particles. At the low loading ratios, the size of the viscous sublayer thickness significantly affect the heat transfer; while at a high loading, the ratio of solid-to-gas heat capacity and specific weight is dominant factor affecting the heat transfer process.

Using an Eulerian–Lagrangian model and considering gas k_θ–ε_θ equations, Avila and Cervantes [4] studied heat transfer coefficients in a pipe with constant wall temperature. They concluded that at low loading ratios two factors could affect the heat transfer. The

* Corresponding author. Tel.: +1-315-268-2322; fax: +1-315-268-6438.
E-mail address: ahmadi@clarkson.edu (G. Ahmadi).

0017-9310/02/$ - see front matter
PII: S0017-9310(01)00234-4

Nomenclature

A	particle surface, m^2
c_p	specific heat, J/kg K
c_d	drag coefficient
D	pipe diameter, m
d	particle diameter, m
F	coefficient in Eq. (14)
f_μ	damping function in Eq. (2)
f_λ	damping function in Eq. (12)
g_0	gravity acceleration, m/s^2
h_p	heat transfer coefficient, W/m^2 K
K	thermal capacity, W/m K
k	turbulent kinetic energy, m^2/s^2
k_θ	temperature variance, $1/2\overline{t't'}$
m	particle mass, kg
Nu	Nusselt number $= Dh_p/K$
P	pressure, N/m^2
Pr	Prandtl number $= \mu c_p/K$
Pr_t	turbulent Prandtl number $= \nu_t/\alpha_t$
q	heat flux, W/m^2
R	pipe radius, m
r	radial coordinate
Re	Reynolds number $= DV\rho/\mu$
Re_p	particle Reynolds number (Eq. (28))
S	source term due to solid phase
T	mean temperature, °C
t'	temperature fluctuation, °C
T^*	friction temperature, $(\alpha/u^*)(\partial T_g/\partial y)_{wall}$
t	time, s
u	velocity, m/s
u'	velocity fluctuation, m/s
u^*	friction velocity, $\sqrt{\nu(\partial U_g/\partial y)_{wall}}$
U	gas means velocity, m/s
x	vertical coordinates, m
y	distance from the wall, m
Z	loading ratio, solid mass flux/gas mass flux

Greek symbols

α	thermal diffusivity, m^2/s
α_t	thermal eddy diffusivity, m K
β	stretching parameter (Eq. (32))
ε	dissipation rate of turbulent kinetic energy, m^2/s^3
ε_θ	dissipation rate of turbulent thermal energy, K^2/s
ϕ	particle volume concentration
μ	viscosity, N s/m^2
ν	kinematic viscosity, m^2/s
ν_t	eddy viscosity, m^2/s
ρ	density, kg/m^3
σ	constant number
τ	turbulence timescale, s
τ_θ	thermal turbulence timescale, s

Subscripts and superscripts

f	fluid
g	gas
k	hydrodynamic intensity
0	single-phase parameter
p	particle
t, θ	thermal turbulence
u	velocity
w	wall
$'$	fluctuating part
$\bar{}$	average value
+	non-dimensional parameter

first is the reduction of heat transfer coefficient due to substantial decrease in turbulence intensity. The second factor is the increase of heat transfer coefficient due to high suspension heat capacity, especially when particle size is small. Rizk et al. [5] modeled the source term due to the solid phase in the fluid k_θ–ε_θ transport equations in an Eulerian approach in terms of particle relaxation time and turbulence timescale. Andreux et al. [6] used an Eulerian–Lagrangian model solving the momentum and energy equations for each phase. They used a turbulent Prandtl number model for gaseous phase, but the model did not perform satisfactorily at high loading ratios.

Using a one-way simulation model, Sommerfeld [7] showed that the particle collision has a significant effect on the particle velocity fluctuation field. Similarly, Mansoori et al. [8] by one-way simulation model showed that the particle interactions and collisions could influences the particle thermal fluctuation intensity. The one-way and two-way coupling simulations of Jaberi [9] showed that the thermal coupling is quite important. The modulation of the fluid and particle temperature fields is not solely due to modification of the fluid velocity field by particles. Furthermore, the thermal transport in two-phase turbulent flows and the thermal interactions between the phases cannot be overlooked in these flows.

Schwab and Lakshminarayana [10] showed that the transport equations of dynamic and thermal turbulence timescales and kinetic energy eliminates the difficulties of numerical problems in single-phase flows and leads to simpler wall boundary condition. Saffar-Avval and co-workers [8,11] investigated the effect of thermal interaction between particles and turbulence temperature field in a vertical gas–solid pipe flow. They introduced the source term due to solid phase in the k_θ–τ_θ transport equations. The model showed that for a fully developed turbulent pipe flow, the solid phase causes thermal

turbulent attenuation, and this effect is more significant for higher mass loading ratios and larger particle diameters. The effect of collision on the thermal turbulence attenuation was also studied in a one-way simulation model. The model predicted that the collision causes the attenuation to be more important in the core region of the pipe.

The provided review of the literature shows that the effect of turbulence–particle interactions on heat transfer in gas–solid flows is not well understood. In this study, flow and heat transfer in a vertical gas–solid turbulent duct flow is studied. The two-way interaction of two-phase flows is included in the Eulerian–Lagrangian model used in the analysis. The k_θ–τ_θ transport equation model, in addition to a k–τ model for two-phase flows are used in the simulation. The case of an upward pipe flow with constant wall heat flux is studied. The results are presented in graphical forms and discussed.

2. Mathematical modeling

In this section the mathematical model for the two-way interaction of gas–solid flows in an Eulerian–Lagrangian approach is presented. Assuming an incompressible and fully developed turbulent gas flow inside a vertical pipe, the mean velocity and temperature fields are evaluated by solving the time-dependent Reynolds averaged-conservation equations. The governing equations are closed with a k–τ model for hydrodynamic simulation and a k_θ–τ_θ model for thermal simulation. The coupling source terms due to solid phase used in the k_θ–τ_θ equations are the extended form of Saffar-Avval et al. [11]

2.1. Hydrodynamic analysis

The equations of turbulent flow field are obtained by applying the Reynolds decomposition on the instantaneous momentum equation. The closed time-dependent equation for the mean gas velocity in a vertical fully developed axisymmetric gas–solid flow in cylindrical coordinates is given as

$$\frac{\mathrm{D}[(1-\phi)U_\mathrm{g}]}{\mathrm{D}t} = \frac{1}{r}\frac{\partial}{\partial r}\left[r(\nu+\nu_\mathrm{t})(1-\phi)\frac{\partial U_\mathrm{g}}{\partial r}\right] - (1-\phi)g_0 - (1-\phi)/\rho_\mathrm{g}\frac{\partial p}{\partial x} + S_u. \quad (1)$$

Here ϕ is the solid volume fraction, S_u is the coupling source term due the interaction of gas and solid and $\nu_\mathrm{t} = c_\mu f_\mu k\tau$ [10] is the eddy viscosity, where coefficient c_μ is 0.09 [12]. The damping function f_μ is given as [10]

$$f_\mu = \left(1 + \frac{3.45}{\sqrt{Re_\mathrm{T}}}\right)\tanh(y^+/70), \quad (2)$$

Here, the turbulence Reynolds number is defined as, $Re_\mathrm{T} = k\tau/\nu$. In Eq. (1), S_u, the coupling source term due to the presence of particle which is given as

$$S_u = \frac{\rho_\mathrm{p}}{\tau_\mathrm{p}\rho_\mathrm{g}}[\phi_\mathrm{p}(U_\mathrm{p} - U_\mathrm{g})], \quad (3)$$

where τ_p is the particle dynamic relaxation time, defined as

$$\tau_\mathrm{p} = \frac{4}{3}\frac{\rho_\mathrm{p} d_\mathrm{p}}{\rho_\mathrm{g} c_\mathrm{d}|U_\mathrm{p} - U_\mathrm{g}|} \quad (4)$$

and c_d is the drag coefficient.

Based on the transport of the fluctuating turbulent velocity field, the transport equations for k–τ for gas–solid flow can be formulated. For single-phase flows, Schwab and Lakshminarayana [10] recommended the use of k–τ model, because of the simplicity in applying the boundary conditions in the numerical procedure. For an axisymmetric fully developed two-phase flow, the resulting k–τ transport equations are given as:

$$\frac{\mathrm{D}(1-\phi)k}{\mathrm{D}t} = \frac{1}{r}\frac{\partial}{\partial r}\left[r(1-\phi)\left(\nu + \frac{\nu_\mathrm{t}}{\sigma_k}\right)\frac{\partial k}{\partial r}\right] + \nu_\mathrm{t}(1-\phi)\left(\frac{\partial U_\mathrm{g}}{\partial r}\right)^2 - (1-\phi)\varepsilon - S_k, \quad (5)$$

$$\frac{\mathrm{D}(1-\phi)\tau}{\mathrm{D}t} = \frac{1}{r}\frac{\partial}{\partial r}\left[r(1-\phi)\left(\nu + \frac{\nu_\mathrm{t}}{\sigma_\tau}\right)\frac{\partial \tau}{\partial r}\right] + c_{\tau 1}(1-\phi) - c_{\tau 2}(1-\phi)\frac{\tau}{k}\nu_\mathrm{t}\left(\frac{\partial U_\mathrm{g}}{\partial r}\right)^2 + \frac{2}{k}(1-\phi) \times \left[\left(\nu + \frac{\nu_\mathrm{t}}{\sigma_\tau}\right)\frac{\partial \tau}{\partial r}\frac{\partial k}{\partial r}\right] - \frac{2}{\tau}(1-\phi) \times \left[\left(\nu + \frac{\nu_\mathrm{t}}{\sigma_\tau}\right)\frac{\partial \tau}{\partial r}\frac{\partial \tau}{\partial r}\right] + S_\tau. \quad (6)$$

The coefficients in Eqs. (5) and (6) are given as $c_{\tau 1} = 0.92$, $c_{\tau 2} = 0.44$ [10], $\sigma_k = 1$ [12] and $\sigma_\tau = 1$. In Eq. (5), S_k is the source term due to the solid phase interaction with gas. i.e.,

$$S_k = -\frac{\rho_\mathrm{p}}{2\rho_\mathrm{g}\tau_\mathrm{p}}\left[\overline{\phi}(\overline{u_i^{\mathrm{p}'}u_i^{\mathrm{g}'}} - \overline{u_i^{\mathrm{g}'}u_i^{\mathrm{g}'}}) + \overline{\phi' u_1^{\mathrm{g}'}}(U_\mathrm{p} - U_\mathrm{g})\right] - \frac{\rho_\mathrm{p}}{2\rho_\mathrm{g}\tau_\mathrm{p}}\left[\overline{\phi' u_i^{\mathrm{g}'}(u_i^{\mathrm{p}'} - u_i^{\mathrm{g}'})}\right]. \quad (7)$$

Here $u_i^{\mathrm{g}'}$ and $u_i^{\mathrm{p}'}$ are, respectively, the fluctuation velocities of gas and particle phases and ϕ' is the particle concentration fluctuation. Neglecting the triple correlation terms, the coupling term becomes

$$S_k = -\frac{\rho_\mathrm{p}}{2\rho_\mathrm{g}\tau_\mathrm{p}}\left[\overline{\phi}(\overline{u_i^{\mathrm{p}'}u_i^{\mathrm{g}'}} - \overline{u_i^{\mathrm{g}'}u_i^{\mathrm{g}'}}) + \overline{\phi' u_1^{\mathrm{g}'}}(U_\mathrm{p} - U_\mathrm{g})\right]. \quad (8)$$

The first term in the right-hand side of Eq. (8) involves the fluid–particle velocity correlation. The second term

shows that the effect of particle and gas mean velocity differences, as well as the particle concentration and velocity correlation.

The source term in Eq. (6) is given as

$$S_\tau = \frac{S_k}{\varepsilon}(c_{\tau 3} - 1). \tag{9}$$

Here, coefficient $c_{\tau 3} = 2.0$ is used.

The gas–particle velocity correlation term $\overline{u_i^{p'} u_i^{g'}}$ in Eq. (8) is evaluated using a combined Eulerian–Lagrangian averaging procedure. First the mean particle velocity, $U_p = U_1^p$, during each Lagrangian time-step is evaluated within a computational control volume (computational cell) around each node by ensemble averaging. Then the cross-correlation term $\overline{u_i^{p'} u_i^{g'}}$ is evaluated by the following averaging procedure:

$$\overline{u_i^{p'} u_i^{g'}} = \frac{1}{\Delta t_E N_p} \sum_{k=1}^{N_t} \sum_{n=1}^{N_p} [(u_i^p - U_i^p)(u_i^g - U_i^g)] \Delta t_L, \tag{10}$$

where u_i^p is the instantaneous particle velocity and u_i^g is the instantaneous gas velocity. Here, N_p is the number of particle in the computational cell, $\Delta t_E = N_t \cdot \Delta t_L$ and N_t is the number of Lagrangian time-steps in each Eulerian time-step. In Eq. (10), the summation over n (and division by N_p) indicates the ensemble averaging over the particles in each computational cell, and the summation over k (and division by N_t) denotes the temporal averaging over the Eulerian time-step.

The particle concentration–gas velocity correlation term is modeled using a gradient transport hypothesis. That is,

$$\overline{\phi' u_1^{'g}} \approx \frac{\nu_t}{\sigma_{pg}} \frac{\partial \overline{\phi}}{\partial r},$$

where σ_{pg} is taken to be a constant equal to 1.

2.2. Thermal analysis

The equation governing the mean turbulent gas temperature is given as

$$\frac{D(1-\phi)T}{Dt} = \frac{1}{r}\frac{\partial}{\partial r}\left[r(1-\phi)(\alpha + \alpha_t)\frac{\partial T}{\partial r}\right] + S_T. \tag{11}$$

The thermal eddy diffusivity is by $\alpha_t = c_\lambda f_\lambda k \tau_\theta$ [10]. Here τ_θ represents thermal time scale, c_λ is a constant, which is assumed to be equal to 0.2, and the damping function f_λ is modeled as [10]

$$f_\lambda = \left(1 + \frac{2.4}{\sqrt{Re_{t\theta}}}\right)\tanh(y^+/120). \tag{12}$$

Here $Re_{t\theta}$ is the turbulent Reynolds number based on k and τ_θ, i.e., $Re_{t\theta} = k\tau_\theta/\nu$. The second term on the right-hand side of Eq. (11) is the coupling term due to the solid phase interaction with the gas. According to [5]

$$S_T = \frac{F}{\rho_g c_{pg}}\left[\phi(T_p - T_g)\right], \tag{13}$$

where

$$F = 6Nu_p K_g / d_p^2. \tag{14}$$

The resulting k_θ–τ_θ transport equations for an axisymmetric fully developed two-phase flow are given as:

$$\frac{D(1-\phi)k_\theta}{Dt} = \frac{1}{r}\frac{\partial}{\partial r}\left[r(1-\phi)\left(\alpha + \frac{\alpha_t}{\sigma_{k\theta}}\right)\frac{\partial k_\theta}{\partial r}\right] + \alpha_t\left(\frac{\partial T_g}{\partial r}\right)^2 - \varepsilon_\theta - S_{k\theta}, \tag{15}$$

$$\begin{aligned}\frac{D(1-\phi)\tau_\theta}{Dt} = {} & \frac{1}{r}\frac{\partial}{\partial r}\left[r(1-\phi)\left(\alpha + \frac{\alpha_t}{\sigma_{\tau\theta}}\right)\frac{\partial \tau_\theta}{\partial r}\right] \\ & + c_{\tau\theta_1}(1-\phi)\frac{\tau_\theta}{k_\theta}\alpha_t\left(\frac{\partial T_g}{\partial r}\right)^2 + c_{\tau\theta 2}(1-\phi) \\ & \times \frac{\tau_\theta}{k}\nu_t\left(\frac{\partial U_g}{\partial r}\right)^2 + (c_{\tau\theta 3} - 1)(1-\phi) \\ & + \frac{2}{k_\theta}(1-\phi)\left[\left(\alpha + \frac{\alpha_t}{\sigma_{\tau\theta}}\right)\frac{\partial \tau_\theta}{\partial r}\frac{\partial k_\theta}{\partial r}\right] \\ & - \frac{2}{\tau_\theta}(1-\phi)\left[\left(\alpha + \frac{\alpha_t}{\sigma_{\tau\theta}}\right)\frac{\partial \tau_\theta}{\partial r}\frac{\partial \tau_\theta}{\partial r}\right] \\ & + c_{\tau\theta 4}(1-\phi)\frac{\tau_\theta}{\tau} + S_{\tau\theta}.\end{aligned} \tag{16}$$

The model coefficients in Eqs. (15) and (16) are evaluated in [10] are:

$$c_{\tau\theta 1} = 0.27, \quad c_{\tau\theta 2} = -0.7,$$
$$c_{\tau\theta 3} = [1 - \exp(-y^+/4.8)]^2,$$
$$c_{\tau\theta 4} = (1.92 - 1)[1 - \exp(-y^+/4.9)]^2.$$

In Eq. (15), $S_{k\theta}$, is the source term due to the solid phase interaction with the gas and is given by

$$\begin{aligned}S_{k\theta} = {} & -\frac{F}{2\rho_g c_{pg}}\left[\overline{\phi}(\overline{t_p' t_g'} - \overline{t_g' t_g'}) + \overline{\phi' t_g'}(T_p - T_g)\right] \\ & - \frac{F}{2\rho_g c_{pg}}\left[\overline{\phi' t_g'}(t_p' - t_g')\right],\end{aligned} \tag{17}$$

where t_g' is the fluctuating gas temperature and t_p' is the fluctuating particle temperature. Neglecting the triple correlation terms, the coupling term simplified to

$$S_{k\theta} = -\frac{F}{2\rho_g c_{pg}}\left[\overline{\phi}(\overline{t_p' t_g'} - \overline{t_g' t_g'}) + \overline{\phi' t_g'}(T_p - T_g)\right]. \tag{18}$$

The first term on the right-hand side of Eq. (18) is the fluid–particle temperature correlation. The effect of particle and gas mean temperatures differences and the particle concentration and gas temperature correlation appears in the second term. The correlation terms

between particle concentration and gas temperature are modeled by a gradient transport hypothesis given as

$$\overline{\phi' t'_{\mathrm{g}}} \approx \frac{\alpha_{\mathrm{t}}}{\sigma_{\mathrm{tg}}} \frac{\partial \overline{\phi}}{\partial r},$$

where $\sigma_{\mathrm{tg}} = 1$ is a constant.

The gas–particle temperature correlation term $\overline{t'_{\mathrm{p}} t'_{\mathrm{g}}}$ in Eq. (18) is evaluated using a combined Eulerian–Lagrangian averaging procedure similar to that used for the gas–particle velocity correlation. First the mean particle temperature, T_{p}, during each Lagrangian time-step is evaluated within a computational control volume (computational cell) around each node by ensemble averaging. Then the cross-correlation $\overline{t'_{\mathrm{p}} t'_{\mathrm{g}}}$ is evaluated by ensemble averaging over the particles in each computational cell and temporal averaging over the Eulerian time-step similar to the procedure described for the velocity cross-correlation.

The last term, in τ_θ-equation is the coupling term due to the presence of the solid phase. This term reflects the effect of particles on the evolution of thermal turbulence timescale. Here it is modeled as the ratio of the coupling term due to the presence of the solid phase to the thermal turbulence dissipation term, i.e.,

$$S_{\tau\theta} = \frac{S_{k\theta}}{\varepsilon_\theta}(c_{\tau\theta} - 1). \tag{19}$$

Here $c_{\tau\theta} = 2.0$ [5] is used.

2.3. Instantaneous turbulence fluctuation

The generation of fluctuating components of fluid velocity using a continuous Gaussian random field model was suggested by Kraichnan [13]. Accordingly, the fluctuation component of the turbulence in an isotropic field is given by

$$\vec{u}'^{+}(\vec{X}^{+}, t^{+}) = \sqrt{\frac{2}{M}} \left\{ \sum_{n}^{M} \vec{U}_1 [\cos(\vec{K}_n \cdot \vec{X}^{+} + \omega_n t^{+})] \right\} + \sqrt{\frac{2}{M}} \left\{ \sum_{n}^{M} \vec{U}_2 [\sin(\vec{K}_n \cdot \vec{X}^{+} + \omega_n t^{+})] \right\}, \tag{20}$$

where $\vec{X}^{+}$ is the position vector and all quantities are nondimensionalized with a velocity scale u^* and kinematic viscosity. That is

$$u_i^{+} = \frac{u_i}{u^*}, \quad t^{+} = \frac{t u^{*2}}{\nu}, \quad x_i^{+} = \frac{x_i u^*}{\nu}. \tag{21}$$

In Eq. (20)

$$\vec{U}_1 = \vec{\zeta}_n \times \vec{K}_n, \tag{22}$$

$$\vec{U}_2 = \vec{\xi}_n \times \vec{K}_n \tag{23}$$

with

$$\vec{K}_n \cdot \vec{U}_1 = \vec{K}_n \cdot \vec{U}_2 = 0. \tag{24}$$

The components of vectors $\vec{\zeta}_n, \vec{\xi}_n$ and frequencies ω_n are picked independently from a Gaussian distribution with a standard deviation of unity. Each component of $\vec{K}_n$ is also a Gaussian random number with a standard deviation of 1/2. In Eq. (20) M is the number of terms in the series. (Here $M = 100$ is used.)

Eq. (20) generates a continuous incompressible Gaussian random field, which resembles an isotropic homogeneous turbulence. For application to non-homogeneous flows a scaling is needed [15,16]. Here a similar scaling is used using the available data for turbulent velocity field [17].

The approach is also extended and used for generating the temperature fluctuations using the experimental data of [10] temperature fluctuation intensities. That is, the nondimensional fluctuation temperature is evaluated from

$$t'^{+}(\vec{X}^{+}, t^{+}) = \sqrt{\frac{2}{M}} \left\{ \sum_{n}^{M} T_1 [\cos(\vec{K}_n \cdot \vec{X}^{+} + \omega_n t^{+})] \right\} + \sqrt{\frac{2}{M}} \left\{ \sum_{n}^{M} T_2 [\sin(\vec{K}_n \cdot \vec{X}^{+} + \omega_n t^{+})] \right\}. \tag{25}$$

Here $t'^{+} = t'_{\mathrm{g}}/t^*$ with t^* being the root-mean square gas temperature fluctuation. All random coefficients in Eq. (26) are generated similar to that of the Kraichnan model for the flow field, except for T_1 and T_2 that are picked from independent Gaussian distributions with a standard deviation of unity.

2.4. Particle Lagrangian simulation

A Lagrangian particle tracking approach is used in the analysis. The equation of motion for a spherical particle including the viscous drag and gravitational forces is given by [18]:

$$\frac{\mathrm{d}u_i^{\mathrm{p}}}{\mathrm{d}t} = \frac{3 c_{\mathrm{d}} \rho_{\mathrm{g}}}{4 d_{\mathrm{p}} \rho_{\mathrm{p}}} |u_i^{\mathrm{g}} - u_i^{\mathrm{p}}| (u_i^{\mathrm{g}} - u_i^{\mathrm{p}}) + g, \tag{26}$$

$$\frac{\mathrm{d}x_i^{\mathrm{p}}}{\mathrm{d}t} = u_i^{\mathrm{p}}. \tag{27}$$

Here u_i^{p} is the particle velocity, u_i^{g} is the instantaneous fluid velocity with $u_i^{\mathrm{g}} = U_i^{\mathrm{g}} + u_i^{\mathrm{g}'}$, where U_i^{g} is the fluid mean velocity and $u_i^{\mathrm{g}'}$ is the fluctuating component. In Eq. (26) c_{d} is the local drag coefficient, which is a function of particle Reynolds number, i.e.,

$$c_{\mathrm{d}} = \frac{24}{Re_{\mathrm{p}}}(1 + Re_{\mathrm{p}}^{0.667}/6), \tag{28}$$

where

$$Re_p = |u_i^g - u_i^p| d_p / v. \quad (29)$$

When a particle strikes a wall, it is assumed that it will bounce from the surface. The rebound velocity of a solid particle from the wall is evaluated using the classical impulse equation for inelastic collisions. Here unless stated otherwise a coefficient of restitution of 0.9 in used.

Thermal energy equation of the particles is given as [12]

$$mc_p \frac{dT^p}{dt} = h_p A (T^g - T^p), \quad (30)$$

where m is the particle mass, c_p is the particle heat capacity, A is the particle surface area and h_p is the heat transfer coefficient. The term on the right-hand side of (30) is due to the gas–particle heat transfer. Here T^p is the particle temperature and T^g is the fluid temperature at the particle location. Note that $T^g = \overline{T^g} + t^{g'}$, where $t^{g'}$ is the gas fluctuating temperature, which is generated using the extended Kraichnan model given by Eq. (25). The convection transfer coefficient h_p is evaluated from the expression given in [12]. That is

$$Nu_p = \frac{h_p d}{k_g} = 2 + 0.6 Re_p^{0.5} Pr^{0.3}, \quad (31)$$

where Nu_p is the Nusselt number, k_g is the gas heat conductivity and Pr is the Prandtl number.

It should be emphasized that the mean gas velocity and temperature are evaluated from the Eulerian field equations. The instantaneous gas velocity and temperature at the particle location are then determined by adding the fluctuation fields as given by Eqs. (20) and (25) to the mean fields. The instantaneous values are then used in Eqs. (26) and (30) for evaluating the particle motion and temperature. The computational procedure and the iterative scheme for accounting for the two-way interactions are described in the following section.

3. Numerical procedures

The time-dependent computations are carried out for a turbulent axisymmetric quasi-fully developed pipe flow with constant heat flux at the wall. An iterative procedure between Eulerian mean flow evaluation and the Lagrangian particle tracking is used to account for the two-way interactions.

To start the solution procedure, the experimentally available data for fully developed single-phase gas flow is used as the initial gas flow condition. The Lagrangian particle trajectory and heat transfer equations are then solved in the known gas velocity and temperature fields, while particle–particle collision is ignored. In this way the uncorrected individual particle locations, velocities and temperatures after each Lagrangian time-step are evaluated. As noted before, averaging over the ensemble of particles and the Eulerian time-step was used to for evaluating the mean and fluctuating velocity and temperature of particles in each control volume cell (around each computational node). The two-way interaction source terms $\overline{u_p' u_g'}$ and $\overline{t_p' t_g'}$ are then evaluated using an averaging procedure described by Eq. (10) within each control volume.

In the next step the Eulerian field equations are modified by addition of the source terms due to presence of particles in the gas. Then the gas transport equations for $U_g, T_g, K, \tau, K_\theta, \tau_\theta$, including the solid-phase interaction source terms are solved. After obtaining the converged solution for gas-phase velocity and temperature and turbulence velocity and thermal intensities, as well as timescales, all particles are tracked again through the newly evaluated flow field and temperatures. For every Eulerian time-step, this iterative procedure is repeated until the convergence is achieved. It should be emphasized that, for this procedure to converge, the Lagrangian time-step must be chosen to be much smaller than the Eulerian time-step. According to [18], the Lagrangian time-step should be chosen to be smaller than 10% of the following timescales:

- The time required for a particle to cross the control volume.
- The particle response time.
- The local timescale of turbulence.

In the present simulations, the Lagrangian particle tracking time-step is selected to be 10 times smaller than the time-step for the Eulerian mean flow computations, which was smaller than the three timescales listed above.

3.1. Boundary and initial conditions

Spherical glass particles are randomly distributed at the entrance region with an initial velocity equal to gas mean velocity and initial mean temperature equal to gas mean temperature. At the wall the following boundary conditions are assumed:

$$U_g = K = K_\theta = \tau = \tau_\theta = 0,$$
$$k_g \frac{\partial T_g}{\partial r} = q_w. \quad (32)$$

At the centerline the symmetric conditions for all variables are imposed.

It should be emphasized that the governing equations for $U_g, K, \tau, K_\theta, \tau_\theta$ are solved in the core region (between the pipe center and a node located at $y^+ = 30$) [6], while gas mean temperature equation is solved in entire region (up to the wall). Therefore, the computational boundary condition at the first grid next to the wall for $U_g, K, \tau, K_\theta, \tau_\theta$ are given as

$$\frac{\partial K}{\partial r}=\frac{\partial K_\theta}{\partial r}=\frac{\partial \tau}{\partial r}=\frac{\partial \tau_\theta}{\partial r}=0.$$

$$\text{For } 5\leqslant y^+\leqslant 30: \quad U^+=5\ln y^+-3.05. \tag{33}$$

$$\text{For } y^+\geqslant 30: \quad U^+=1/0.4\ln y^+ +5.7.$$

That is, the law of the wall for the velocity field is used.

As noted before, to properly account for the heat transfer, the temperature equation was solved up to the wall, and the heat flux boundary condition given by Eq. (32) was used. The needed valued of $U_g, K, \tau, K_\theta, \tau_\theta$ for temperature calculation near the wall is obtained by an interpolation scheme between the wall values given in Eq. (32) and the calculated values at the first grid from the wall (at about $y^+=30$).

To increase the accuracy of temperature field close to the wall, the grid generation scheme is chosen to be finer near the wall. The mesh size is small near the wall and becomes larger with distance from the wall. This was achieved using the stretching scheme suggested in [19]. That is

$$y(\text{comp})=1-\frac{\ln\{[\beta+1-(y/R)]/[\beta-1+(y/R)]\}}{\ln[(\beta+1)/(\beta-1)]}, \tag{34}$$

where β is the stretching parameter that must be greater than 1. The stretching transformation clusters more point near the wall as β approaches 1. Here β is chosen as 1.01.

For evaluating particle trajectories and temperatures, a periodic boundary condition is assumed. That is for each particle, which leaves the computational domain, another particle is assumed to enter from the opposite side with the same velocity and temperature. Particles are also assumed to rebound the wall with a restitution coefficient of 0.9.

When the particle is close to the wall, the heat transfer through the gas lens between particle and wall is accounted for in the simulation. For this purpose the model described by Mansoori et al. [20] is used. When the particle is sufficiently close to the wall, heat conduction through the gas lens between particle and wall is computed, ignoring the gas movement in the lens. The heat conduction through the solid material during the short contact time between the particle and the wall, which is negligibly small, is ignored.

4. Numerical validation

In the absence of the experimental data for combined hydrodynamic and thermal multiphase flow conditions, the validations of computational approach are carried out for a two-phase gas–solid flows and a heat transfer case.

4.1. Velocity field

Experimental data of Tsuji et al. [14] were used to validate the hydrodynamic part of computational model. The experimental data of Tsuji et al. [14] for a mass loading ratio (solid mass flux/gas mass flux) of 1.13, and gas Reynolds number of 32 000 in a vertical pipe of 30.5 mm inner diameter are reproduced in Fig. 1. In the experiment the gas centerline velocity was 18.9 m/s and the particles were polystyrene spheres with a density of 1020 kg/m^3 and a diameter of 200 μm. Using the Eulerian–Lagrangian computational model, the gas particle flows for the condition of Tsuji et al. [14] is simulated and results are plotted in Fig. 1. Fig. 1 shows that the predicted mean gas and particle velocities are in good agreement with the experimental data.

Fig. 2 compares the simulated particulate turbulence intensity with the experimental data of Tsuji et al. [14] for a mass loading ratio of 1.3. In this figure, the solid squares represent the experiment data. This figure shows that the model predictions for the particulate turbulence intensity are in good agreement with the experimental data.

4.2. Temperature field

In this section comparison of the numerical predictions with the experimental data of Depew and Farber [21] are presented. Depew and Farber [21] measured the variation of the mean suspension heat transfer coefficient with the mass loading ratio, Z. Their experiment was performed for a vertical pipe flow with a diameter of 0.019 m, with a constant wall heat flux. The fluid medium was air containing glass spherical particles with a diameter of 200 μm and a gas Reynolds number of 13 500.

Fig. 3 shows the comparison of the model predictions with the experimental data of [21] at a length/diameter

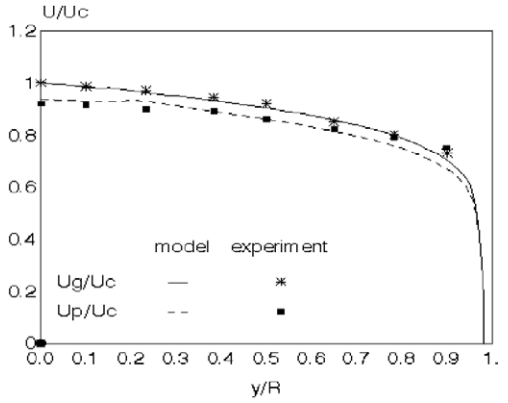

Fig. 1. Gas and particle velocity profiles at mass loading ratio of $Z=1.13$. Comparison with the experimental data of Tsuji et al. [14] for $d_p=200$ μm and $Re=32000$.

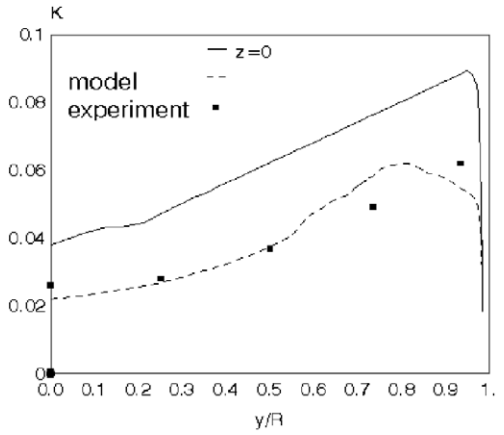

Fig. 2. Comparison of gas turbulence intensity for mass loading ratio of $Z = 1.3$ with data of Tsuji et al. [14] for $d_p = 200$ μm and $Re = 32000$.

ratio of $x/D = 46.4$. At this length/diameter ratio, a fully developed condition may be assumed to prevailed in the pipe. Here, the suspension Nusselt number is given by

$$Nu = \frac{2Rq_w}{k_g(T_w - T_m)}, \tag{35}$$

where T_m is the mean suspension temperature, which is evaluated as

$$T_m = \frac{\int c_{pg}\rho_g(1-\phi)U_g T_g \, dA + \int c_{pp}\rho_p \phi U_p T_p \, dA}{\int c_{pg}\rho_g(1-\phi)U_g \, dA + \int c_{pp}\rho_p \phi U_p \, dA}. \tag{36}$$

The thermal conductivity of gas is computed at the film temperature $(T_m + T_w)/2$. Heat transfer coefficient for single-phase gas flow is evaluated using a well established correlation [22],

$$Nu_0 = 0.023 Re^{0.8} Pr^{0.4}. \tag{37}$$

Fig. 3 shows good agreement between the model prediction for the heat transfer coefficient and the experimental data of Depew and Farber [21].

5. Results and discussions

It is well-known that the average heat transfer coefficient for suspension flows increase or decrease by the presence of the particles. Earlier theoretical and experimental studies concluded that different behavior of heat transfer coefficient is mainly due to the decrease of turbulence intensity and/or increase in the suspension heat capacity. Although the importance of turbulence intensity and the suspension heat capacity have been identified, the rather complicated nature of heat transfer mechanisms in two-phase gas–solid flows has not been well-understood [4].

The present model improves the existing two-phase heat transfer models by accounting for the effect of thermal turbulence intensity. As noted before, the present model uses k_θ–τ_θ equations in addition to the k–τ model equations. Using the k–τ model is recommended due to more realistic wall boundary conditions comparing with the k–ε model. As was noted in [10], different value of ε at wall was used by various authors, but the wall boundary condition of $\tau = 0$ is rather precise.

Fig. 4 compares the present model predictions with the experimental results of Jepson et al. [23]. It is seen that model is in reasonable agreement with the experimental data. Here the pipe diameter is 0.038 m and wall

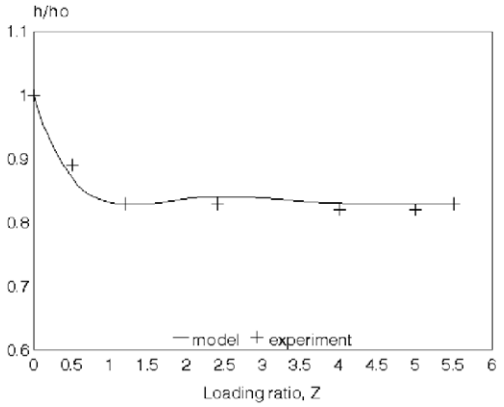

Fig. 3. Predicted ratio of suspension heat transfer coefficient to gas heat transfer coefficient. Comparison with the experimental data of Depew and Farber [21] for $d_p = 200$ μm and $Re = 13500$.

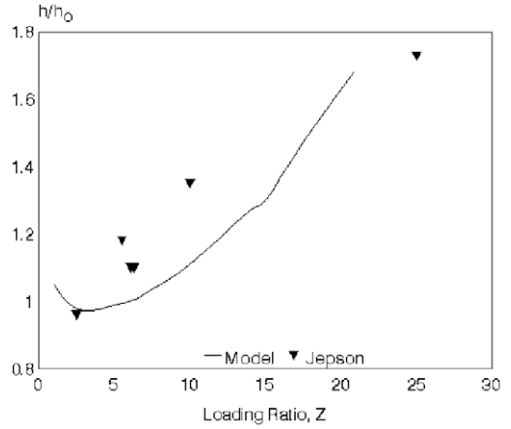

Fig. 4. Variation of ratio of suspension heat transfer coefficient to single-phase gas versus mass loading ratio for $d_p = 200$ μm and $Re = 23000$. (Solid line: present model, symbols: experimental data of Jepson et al. [23].)

heat transfer rate is $q_w = 630\ W/m^2$. The gas superficial velocity is 9 m/s and the particles are sand with $d_p = 200\ \mu m$. It is seen that the heat transfer coefficient is minimum at $Z = 3$. The discrepancy between the model prediction and the experiment is, in part, due to the fact that the experimental data were for the overall heat transfer coefficient; while in the present numerical simulation was for a fully developed condition.

To provide an understanding to the variation of the heat transfer coefficient with loading, the variation of turbulence thermal intensities around the minimum point of heat transfer is studied. For several mass loading ratios between 0 and 5, variations of turbulence thermal intensity across the pipe are shown in Fig. 5. Here the thermal turbulence intensity is nondimensionalized with aid of the friction temperature T^*. The experimental condition of Jepson et al. [23] with particle diameter of 200 μm are also used in these simulations. This figure shows the attenuation of temperature fluctuation near the wall with the presence of solid particles. While the overall temperature fluctuation intensity near the wall decreases, k_θ is higher than the single-phase gas flow intensity in the core region except for mass loading of $Z = 3$. Fig. 5 shows that k_θ in the core region reaches to its minimum for the mass loading ratio for which the heat transfer coefficient is minimum.

The variation of the net thermal dissipation/source term ($\varepsilon_\theta + S_{k\theta}$) in Eq. (14) for different mass loading ratios are shown in Fig. 6. Here the lines present the least square fit to the simulation results. This figure shows that for mass loading ratios of 1 and 5, the net dissipation/source term is negative in the core region but positive near the wall. That is, the thermal fluctuation generated by the particle is larger than the thermal dissipation in the pipe core region and the net dissipation/source term acts to generate gas temperature fluctuation. Near the wall, however, the term $\varepsilon_\theta + S_{k\theta}$ is, generally, positive that leads to dissipation of k_θ. Fig. 6 shows that the net dissipation/source term is positive in the entire region at the point of minimum heat transfer coefficient, for the mass loading ratio of $Z = 3$. The positive value of the net dissipation/source term for $Z = 3$ indicates that it causes attenuation of the temperature fluctuation across the pipe. Figs. 5 and 6 also indicate that at the point of minimum heat transfer coefficient, the solid particles cause the gas temperature fluctuations to be reduced across the entire the pipe cross-section.

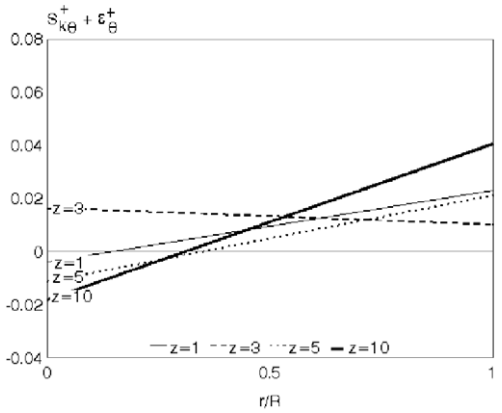

Fig. 6. Variation of total turbulence net thermal dissipation/source term for different mass loading ratios for $d_p = 200\ \mu m$ and $Re = 23000$. ($Z = 1$, solid line; $Z = 3$, dashed line; $Z = 5$, dotted line; $Z = 10$, heavy solid line.)

For a mass loading ratio of 4 and Reynolds number of 23 000, variations of thermal turbulent intensity for different particle diameters are shown in Fig. 7. The geometry is the same as that of experimental study of Jepson et al. [23]. It is seen that the presence of particles attenuate gas temperature fluctuations near the wall, while increase it in the core region. The amount of at-

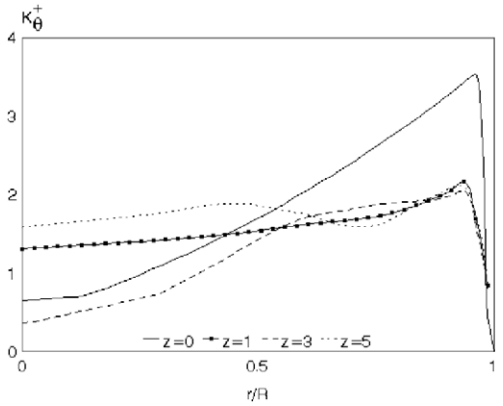

Fig. 5. Turbulence thermal intensity variation for different mass loading ratios for $d_p = 200\ \mu m$ and $Re = 23000$.

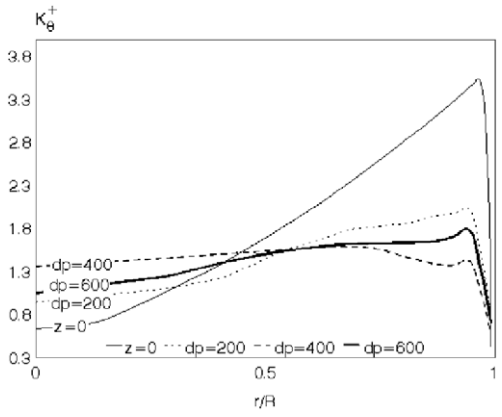

Fig. 7. Gas thermal turbulence intensity variations for various particle diameters for a mass loading of $Z = 4$ and $Re = 23000$.

tenuation near the wall increases as the particle diameter increases from 200 μm to 400 μm, but decreases as particle size further increases. For 400 μm particles, the attenuation in the wall region is so high that the peak gas temperature fluctuations moves away from the wall.

For a mass loading of $Z = 4$, Fig. 8 compares the variation of the heat transfer coefficient with particle diameter with the experimental data of Jepson et al. [23]. Here the suspension heat transfer coefficient is normalized with the respect to that of the single-phase gas flow. It is seen that the heat transfer ratio has a U-shape variation and is larger than one for large and small particles. The suspension heat transfer coefficient reaches to its minimum value for particle diameters of about 400–500 μm. Fig. 8 also shows that the model prediction is in good agreement with the observation of Jepson et al. [23]. The minimum of heat transfer coefficient in Fig. 8 for 400 μm particles appear to coincide with the minimum thermal intensity near the wall in Fig. 7 for the same size particles. This implies that the heat transfer coefficient is well correlated with the thermal turbulence intensity in the range of particle size and mass loading ratio studied.

Variations of turbulence Prandtl, Pr_t, (the ratio of kinematic eddy viscosity to thermal eddy diffusivity) across the pipe as a function of mass loading ratio are shown in Fig. 9. It is seen that the Prandtl number for the suspension is much lower than that of the single-phase gas flow. Values of Pr_t in the wall and in the core regions grows as the loading ratio increase to from 1 to 3 and then it decreases as the loading ratio further increases. This observation further shows that consideration of the effects of thermal turbulence field is important for analyzing heat conducting two-phase flows. This will improve the model prediction capability due to providing the ability to account for the variation

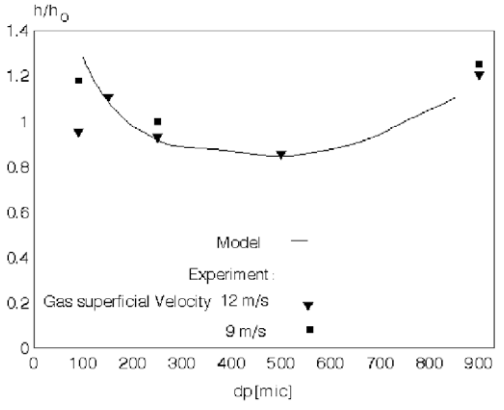

Fig. 8. The distribution of the ratio of suspension to gas heat transfer coefficient for various particle diameters for a mass loading ratio of $Z = 4$ and $Re = 23000$. The symbols show the experimental data of [23] for different gas superficial velocities.

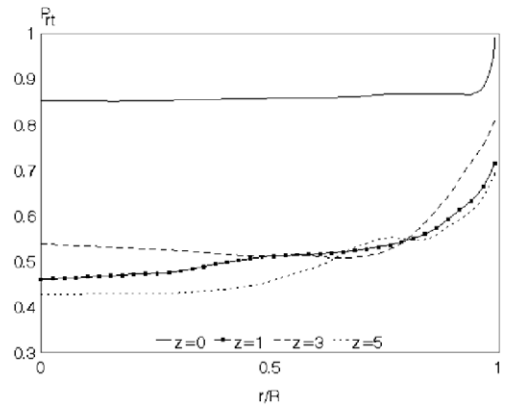

Fig. 9. Variation of turbulent Prandtl number in the radial direction for the gas phase for different mass loading ratios, for $d_p = 200$ μm and $Re = 23000$.

of turbulence Prandtl number. Fig. 9 also shows that use of single-phase gas turbulence Prandtl number and/or a constant Prandtl number as was done earlier [4,6] is unacceptable. While the amount of error may be smaller near the wall, far from the wall region the error could become quite large.

Fig. 10 shows the variation of gas turbulence Prandtl number with particle diameter. This figure shows that the particle size plays an important role on the behavior of Pr_t. The turbulence Prandtl number near the wall is highest for the 400 μm particles, while it is lowest in the core region. Trends of behavior of Pr_t in Fig. 10 are comparable to the inverse of k_θ shown in Fig. 7. These show that both the gas temperature fluctuations and ratio of the rate of heat transfer to the momentum transfer are lowest near the wall region for 400 μm particles for a mass loading of $Z = 4$.

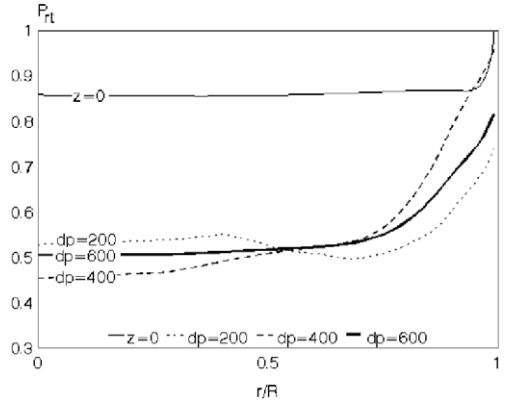

Fig. 10. Variation of turbulent Prandtl number for various particle diameters, for $Z = 4$ and $Re = 23000$.

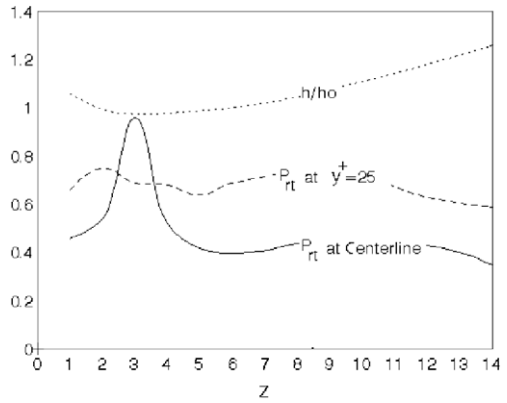

Fig. 11. Variation of turbulent Prandtl number for various mass loading ratios At the center and near the wall for $d_p = 200$ μm and $Re = 23000$.

For $d_p = 200$ μm and $Re = 23000$, variations of turbulence Prandtl number near the wall and at the pipe center line with mass loading ratio are shown in Fig. 11. It is seen that the Prandtl number near the wall varies around 0.7 for a range of mass loading ratios and decreases to about 0.6 for $Z = 14$. The Prandtl number near the centerline, however, has a noticeable peak for the mass loading of about 3. The variation of the heat transfer coefficient is also reproduced in this figure for comparison. Fig. 11 shows that the minimum heat transfer ratio occur when the Prandtl number reaches to its maximum.

6. Conclusions

A new model for analyzing heat transfer in turbulent two-phase gas–solid flows was developed. The model is based on two-way interaction of two-phase flows in an Eulerian/Lagrangian formulation. The model includes the effect of thermal turbulence fluctuations and presents new k_θ–τ_θ model equations, in addition to the k–τ model for two-phase flows. Thus, the thermal eddy diffusivity is directly evaluated from the gas thermal turbulence intensity field. The coupling source terms in the thermal turbulent gas phase equations due to the presence of the solid phase is introduced. The source term in k_θ equation is consisted of two main parts. One part is due to the difference between the mean temperatures of gas and solid phases, and the correlation between the particle concentration fluctuation and the temperature. The other term includes the correlation term between the gas and solid fluctuating temperatures. The model also directly evaluates the turbulence Prandtl number. The new model was used and computer simulations were performed and the mechanisms that control the behavior of suspension heat transfer coefficient especially near its minimum point was studied. Numerical model validation was performed for an upward pipe gas–solid flow with constant wall heat flux. On the basis of the results presented the following conclusions are drawn:

- The simulation results are in good agreement with the available experimental data.
- The heat transfer coefficient for two-phase flows varies with flow Reynolds number, mass loading and particle size.
- The gas turbulence Prandtl number depends on mass loading ratio, flow Reynolds number and particle diameter.
- The model simulation results show that the solid phase causes thermal turbulence fluctuation to attenuate near the wall.
- For the range of Reynolds numbers and particle sizes studied, the heat transfer coefficient appears to have a minimum at a certain mass loading ratio. The minimum heat transfer coefficient appears to occur at the range of mass loading ratio for which the temperature fluctuation near wall also reaches to a minimum.

Acknowledgements

The work of GA was supported by the US Department of Energy, National Energy Technology Laboratory (NETL).

References

[1] T. Yokomine, A. Shimizu, Prediction of turbulence modulation by using κ–ε model for gas–solid flow, in: Advances in Multiphase flow 1995, Elsevier, Amsterdam, 1995, pp. 191–199.
[2] A. Berlemont, M.S. Grancher, G. Gouesbet, Heat and mass coupling between vaporizing droplets and turbulence using a Lagrangian approach, Int. J. Heat Mass Transfer 38 (16) (1995) 3023–3034.
[3] K.S. Han, H.J. Sung, M.K. Chung, Analysis of heat transfer in a pipe carrying two-phase gas–particle suspension, Int. J. Heat Mass Transfer 34 (4) (1991) 69–78.
[4] R. Avila, J. Cervantes, Analysis of the heat transfer coefficient in a turbulent particle pipe flow, Int. J. Heat Mass Transfer 38 (11) (1995) 1923–1932.
[5] M.A. Rizk, A. Torki, M. El-Sallak, A. Mobarak, Mathematical modeling of heat transfer to gas–solid turbulent flows, in: FED, Gas–Particle Flows, ASME, vol. 228, 1995, pp. 327–334.
[6] R. Andreux, P. Boulet, B. Oeserle, Test of an Eulerian–Lagrangian simulation of wall heat transfer in a gas–solid pipe flow, in: W. Rodi, D. Laurence (Eds.), Engineering Turbulence Modeling and Experiments – 4, Elsevier, Amsterdam, 1999, pp. 913–922.
[7] M. Sommerfeld, The importance of inter-particle collisions in horizontal gas–solid channel flows, in: ASME, FED, vol. 228, 1995, pp. 335–345.

[8] Z. Mansoori, M. Saffar-Avval, H. Basirat-Tabrizi, The effect of particle–particle interaction on heat transfer in a horizontal turbulent gas–solid channel flow, in: M.S. Loknath, B. Basu (Eds.), Proceedings of the 4th ISHMT/ASME Heat and Mass Transfer Conference, India, 2000, pp. 379–384.

[9] F.A. Jaberi, Temperature fluctuations in particle-laden homogeneous turbulent flows, Int. J. Heat Mass Transfer 41 (1998) 4081–4093.

[10] J.R. Schwab, B. Lakshminarayana, Dynamic and thermal turbulent time scale modeling for wall bounded shear flows, in: ASME, HTD. Vol. 318, Heat Transfer in Turbulent Flows, 1995, pp. 111–118.

[11] M. Saffar-Avval, H. Basirat Tabrizi, Z. Mansoori, The interparticle effect on turbulent heat transfer in a gas–solid flow, in: G.K. Wolf (Ed.), ASME/ESDA, SWISS 2000, pp. 549–554.

[12] C. Crowe, M. Sommerfeld, Y. Tsuji, Multiphase Flows with Droplets and Particles, CRC Press, Boca Raton, 1998.

[13] H. Kraichnan, Diffusion by random velocity field, Phys. Fluid 11 (1970) 22–31.

[14] Y. Tsuji, Y. Morikawa, H. Shiomi, LDV measurements of an air–solid two-phase flow in a vertical pipe, J. Fluid Mech. 139 (1984) 417–434.

[15] A. Li, G. Ahmadi, Computer simulation of deposition of aerosols in a turbulent channel flow with rough walls, Aerosol Sci. Technol. 18 (1993) 11–24.

[16] A. Li, G. Ahmadi, Aerosol particle deposition with electrostatic attraction in a turbulent channel flow, J. Colloid Interf. Sci. 158 (1993) 476–482.

[17] M. Soltani, G. Ahmadi, Direct numerical simulation of particle entertainment in turbulent channel flow, Phys. Fluids 7 (3) (1995) 647–657.

[18] S. Lain, D. Broder, M. Sommerfeld, Experimental and numerical studies of the hydrodynamics in a bubble column, Chem. Eng. Sci. 54 (1999) 4913–4920.

[19] D.A. Anderson, J.C. Tannehill, R.H. Pletcher, Computational Fluid Mechanics and Heat Transfer, Hemisphere Publishing Corporation, New York, 1984.

[20] Z. Mansoori, M. Saffar-Avval, H. Basirat, Modeling of heat transfer in gas–solid bed, in: TIEES-98, 1998, pp. 120–124.

[21] C.A. Depew, L. Farber, Heat transfer to pneumatically conveyed glass particles of fixed size, Trans. ASME, Series C, J. Heat Transfer 85 (1963) 164–172.

[22] R.G. Boothroyd, H. Haque, Fully developed heat transfer to a gaseous suspension of particles flowing turbulently in ducts of different size, J. Mech. Eng. Sci. 12 (3) (1970) 191–200.

[23] G. Jepson, A. Poll, W. Smith, Heat transfer from gas to wall in a gas/solids transport line, Trans. Inst. Chem. Eng. 41 (1963) 207–211.